# Cohesive energy curves for noble gas solids calculated by adiabatic connection fluctuation-dissipation theory

Judith Harl and Georg Kresse*
*Faculty of Physics and Center for Computational Materials Science, Universität Wien, Sensengasse 8/12, A-1090 Wien, Austria*
(Received 26 September 2007; published 31 January 2008)

We present first-principles calculations for the fcc noble gas solids Ne, Ar, and Kr applying the adiabatic connection fluctuation-dissipation theorem (ACFDT) to evaluate the correlation energy. The ACFDT allows us to describe long-range correlation effects including London dispersion or van der Waals interaction on top of conventional density functional theory calculations. Even within the random phase approximation, the typical $1/V^2$ volume dependence for the cohesive energy of the noble gas solids is reproduced, and equilibrium cohesive energies and lattice constants are improved compared to density functional theory calculations. Furthermore, we present atomization energies for $H_2$, $N_2$, and $O_2$ within the same post-density-functional-theory framework, finding an excellent agreement with previously published data.

DOI: 10.1103/PhysRevB.77.045136 PACS number(s): 71.10.−w, 71.15.Mb, 31.15.V−, 71.45.Gm

## I. INTRODUCTION

Kohn-Sham (KS) density functional theory[1] provides an efficient method to calculate ground-state properties for a wide range of materials. The basis of every KS energy functional is the approximation to the exchange-correlation energy, which should include all many-body energy contributions beyond the Hartree level. The most common choices for the exchange-correlation energy functionals are the local density approximation (LDA) and the generalized gradient approximation (GGA). In particular, the latter yields reasonable results for a large variety of applications, but the local nature of these approximations remains a fundamental drawback for the treatment of van der Waals (vdW) bonded systems. Including exact exchange within generalized KS density functional theory[2] (as, e.g., done in hybrid functionals) does not remedy this failure because a correct description of the vdW interaction relies on the treatment of long-range dynamic correlation effects.

A formalism that provides (in principle) an exact expression for the correlation functional is given by the adiabatic connection fluctuation-dissipation theorem (ACFDT). It relates the exchange-correlation energy to the electronic response of a system with electron density $n(\mathbf{r})$ when continuously switching from the Kohn-Sham Hamiltonian to the exact many-body electron-electron interaction. The response function can be (approximately) evaluated within the framework of time dependent density functional theory. The ACFDT is more than 30 years old,[3–5] and similar concepts within the many-body perturbation formalism go even further back. For instance, the total energy given by the Klein functional[6] on the *GW* level equals the energy resulting from ACFDT within the random phase approximation (RPA).[7] This energy has been evaluated for the jellium bulk[8] and for jellium surfaces.[5,9–11] Nevertheless, the calculation of total energies for realistic systems—whether within the ACFDT or the many-body perturbation formalism—remained impracticable until recently. First ACFDT calculations on total energies of molecules by Furche[12] within the RPA and the RPA+ (Ref. 13) were followed by a number of publications presenting energies and dissociation curves for molecules[7,14–19] and extended systems.[20–22]

In the present work, we focus on the noble gas fcc crystals Ne, Ar, and Kr, the most prominent examples of extended vdW bonded systems. The description of London dispersion or vdW forces between molecules and within extended systems has been subject to numerous publications in the recent years (see, e.g., Refs. 9 and 23–29). The main issue is how to include dispersion forces in an *ab initio* framework without dramatically increasing the computational cost. For the noble gas solids considered in the present work, a coupled-cluster approach with single and double excitations and perturbative triples, as performed by Rościszewski *et al.*,[30] yields results close to experiment. Nevertheless, for extended systems this method is involved so that it remains desirable to find faster methods based on Hartree-Fock (HF) or density functional theory (DFT) to achieve at least an approximated description of the vdW interaction.

Efforts to include dispersion forces in first-principles calculations can be generally divided into two classes. On one hand, a semiempirical long-range vdW interaction can be added on top of an *ab initio* calculation. It is realized by the inclusion of pairwise potentials of the form $C_6^{(ab)}/R_{(ab)}^6$ acting between atom $a$ and atom $b$ separated by the distance $R_{(ab)}$. For the noble gas solids, an example for such a semiempirical treatment can be found in Ref. 27. Although these methods provide an economical way to include dispersion forces, it has been shown by Dobson *et al.* that these methods fail even qualitatively for specific metal geometries.[31,32]

The already discussed ACFDT approach belongs to the class of so called *seamless vdW formalisms*[11] because it includes long-range dispersion forces and at the same time remains reasonably accurate for overlapping electron densities. Even within the RPA, ACFDT has been shown to reproduce the correct qualitative decay for the exchange-correlation potential—therefore also including a vdW-like interaction—although coefficients are influenced by the applied approximations.[33,34]

We will focus on the evaluation of RPA-ACFDT energy-volume curves for the noble gas solids Ne, Ar, and Kr. The resulting equilibrium lattice constants and cohesive energies are compared to experimental, DFT-LDA, and DFT-GGA values. Atomization energies obtained for noble gas

 

molecules[12,16] already indicate that the RPA-ACFDT cohesive energies for the noble gas solids will not be in perfect agreement with experiment. Nevertheless, still the noble gas crystals with their shallow binding energies remain an important test case for both the computational as well as fundamental aspects of the ACFDT. In Secs. II and III, we will present the formalism of ACFDT and shortly describe the technical details of the implementation. Section IV will show test calculations for a small set of molecules. This is done in order to test the implementation and the performance of the ACFDT routines for molecular systems. In Sec. V, we will investigate the ACFDT total energies for the noble gas solids.

## II. TECHNICAL DETAILS

In the following section, we will briefly recapture the main formulas of the adiabatic connection fluctuation-dissipation theorem. For more details, we refer to the first ACFDT papers.[3–5] More recent publications about the theoretical aspects of the ACFDT and its relation to many-body perturbation theory can be found, e.g., in Refs. 19 and 33. Within the ACFDT formalism, the energy $E[n]$ of an interacting electron system with density $n(\mathbf{r})$ is given by

$$E[n] = T_{KS}[\{\psi_i\}] + E_H[n] + E_x[\{\psi_i\}] + E_{\text{ion-el}}[n] + E_c, \quad (1)$$

with the kinetic energy term $T_{KS}$ evaluated for the one-electron KS wave functions $\{\psi_i\}$, the Hartree energy $E_H[n]$, the exchange energy $E_x[\{\psi_i\}]$, and the correlation energy functional $E_c$. The latter can be expressed as a quantity depending on the density-density response function of a series of virtual systems that interact via the scaled Coulomb interaction $\lambda\nu$. The $\lambda$ coupling constant integral over the difference between the frequency response function of the $\lambda$-interacting system, $\chi^\lambda(\mathbf{q},i\omega)$, and that of the respective KS system, $\chi^0(\mathbf{q},i\omega)$, results in the ACFDT expression for the correlation energy

$$E_c = -\int_0^1 d\lambda \int_0^\infty \frac{d\omega}{2\pi} \text{Tr}\{\nu[\chi^\lambda(i\omega) - \chi^0(i\omega)]\}, \quad (2)$$

with

$$\text{Tr}\{AB\} := \sum_{\mathbf{q}\in BZ} g_{\mathbf{q}} \sum_{\substack{|\mathbf{G}+\mathbf{q}|,|\mathbf{G}'+\mathbf{q}| \\ <G_{\text{cut}}^{\chi}}} A_{\mathbf{G}\mathbf{G}'}(\mathbf{q}) B_{\mathbf{G}'\mathbf{G}}(\mathbf{q}). \quad (3)$$

The expression for $E_c$ is formulated in reciprocal space as a dicretized integral over the Brillouin zone (BZ), and a summation over reciprocal lattice vectors, where $\nu_{\mathbf{G},\mathbf{G}'}(\mathbf{q}) = 4\pi e^2 \delta_{\mathbf{G},\mathbf{G}'}/|\mathbf{G}+\mathbf{q}|^2$ denotes the Coulomb kernel in Fourier space. The $k$-point weights $g_{\mathbf{q}}$ are chosen to generate the correct BZ sampling for a given set of $k$ points, and they sum to 1. This formulation follows closely the implementation of the ACFDT in plane-wave codes.

The correlation energy as presented in Eq. (2) is *exact*. However, in order to evaluate the response function of the $\lambda$-interacting system, the Dyson equation[35,36] has to be solved,

$$\chi^\lambda(\mathbf{q}) = \chi^0(\mathbf{q}) + \chi^0(\mathbf{q})[\lambda\nu(\mathbf{q}) + f_{xc}^\lambda(\mathbf{q},i\omega)]\chi^\lambda(\mathbf{q}). \quad (4)$$

Here, $\nu$ and $f_{xc}$ are the Coulomb and the exchange-correlation kernel. The solution of Eq. (4) requires some approximation for the exchange-correlation kernel $f_{xc}$. As done in most of the present ACFDT calculations, we have chosen $f_{xc}=0$, an approximation commonly referred to as RPA. The RPA will lead to perceivable errors, as can already be seen when comparing the RPA to the exact quantum Monte Carlo correlation energies of jellium.[37] A summary about the behavior of other approximations for the exchange-correlation kernel is discussed for jellium in Ref. 38, for jellium slabs in Ref. 39, and for jellium clusters in Ref. 22. However, the inclusion of more sophisticated kernels for inhomogeneous systems is demanding, and simple approximations beyond RPA do not always improve the energetics.[14]

The independent-particle response function $\chi^0$ (the response of the KS system) at imaginary frequencies is given by the expression of Adler[40] and Wiser[41]

$$\chi^0_{\mathbf{G}\mathbf{G}'}(\mathbf{q},i\omega) = \frac{1}{V}\sum_{n,n',\mathbf{k}} 2g_{\mathbf{k}}(f_{n'\mathbf{k}+\mathbf{q}} - f_{n\mathbf{k}}) \times \frac{\langle\psi_{n'\mathbf{k}+\mathbf{q}}|e^{i(\mathbf{q}+\mathbf{G})\mathbf{r}}|\psi_{n\mathbf{k}}\rangle\langle\psi_{n\mathbf{k}}|e^{-i(\mathbf{q}+\mathbf{G}')\mathbf{r}}|\psi_{n'\mathbf{k}+\mathbf{q}}\rangle}{\epsilon_{n'\mathbf{k}+\mathbf{q}} - \epsilon_{n\mathbf{k}} - i\omega}, \quad (5)$$

where $\psi_{n\mathbf{k}}$ and $\epsilon_{n\mathbf{k}}$ are the KS one-electron wave functions and energies of band $n$ and crystal momentum vector $\mathbf{k}$, which lies within the Brillouin zone of the primitive cell with volume $V$. The summation is performed over all occupied and unoccupied bands $n$ and $n'$, and the occupation number is described by the function $f_{n\mathbf{k}}$, which is 1 if the respective band is occupied and 0 otherwise.

The calculation of the ACFDT total energy as given by Eq. (1) is performed using the Vienna *ab initio* simulation package (VASP).[42,43] Within this plane-wave basis set code, the interaction between the ionic cores and the valence electrons is described by the projector-augmented wave (PAW)[44] method in the implementation of Kresse and Joubert.[45] The technical details concerning the optical routines within VASP are presented in Refs. 46 and 47. For the present calculations, the exact all-electron charge density is restored on the plane-wave grid whenever contributions to the correlation energy are evaluated. Details will be presented elsewhere.[48]

The total ACFDT energy $E[n]$ can be separated into two contributions. One part of the total energy results from the evaluation of the HF Hamiltonian at the one-electron KS wave functions $T_{KS}[\{\psi_i\}]+E_H[n]+E_x[\{\psi_i\}]+E_{\text{ion-el}}[n]$, in the following simply referred to as HF energy. The other part is the correlation energy $E_c$ described within the ACFDT framework. These two parts of the total energy, the HF energy and the ACFDT correlation energy, are converged independently with respect to the number of $k$ points and the energy cutoff $E_{\text{cut}}$, which determines the size of the plane-wave basis set for the wave functions.

For the calculation of the correlation energy, special PAW potentials were constructed, describing the scattering properties very accurately up to ~10 Ry above the vacuum level

TABLE I. Core radii $r_c$ for the PAW potentials used in the present work. For nitrogen and oxygen, different potentials have been applied for the evaluation of DFT and HF energies and the calculation of the ACFDT correlation energy. If the core radii differ for specific quantum numbers, they are specified for each channel using subscripts.

| | Valence | $r_c$ (PBE, HF) (a.u.) | $r_c$ (ACFDT-corr) (a.u.) | $E_{\text{cut}}$ (ACFDT-corr) (eV) |
|---|---|---|---|---|
| H | $1s$ | 1.1 | 1.1 | 600 |
| N | $2s2p$ | 1.1 | $1.2_s\ 1.5_{pd}$ | 600 |
| O | $2s2p$ | 1.1 | $1.2_s\ 1.5_{pd}$ | 600 |
| Ne | $2s2p$ | $1.4_s\ 1.8_{pd}$ | $1.4_s\ 1.8_{pd}$ | 650 |
| Ar | $3s3p$ | $1.5_s\ 1.9_{pdf}$ | $1.5_s\ 1.9_{pdf}$ | 390 |
| Kr | $4s4p$ | $1.8_s\ 2.3_{pdf}$ | $1.8_s\ 2.3_{pdf}$ | 340 |

(see Ref. 47). The PAW parameters are summarized in Table I. For the HF and DFT calculations of $N_2$ and $O_2$, the same small core potentials as in Ref. 50 were used to allow an accurate treatment of the dimers with their short bonds. For the correlation energy, such small core potentials do not seem to be required, as demonstrated below (see Table II).

For the determination of the KS wave functions (wave functions and eigenvalues) that are needed as an input for the HF (correlation) energy, the "true" KS exchange-correlation potential should be used, in principle. In fact, if this potential were known, no ACFDT calculations would have to be performed. In the present work, we therefore use either the LDA or the GGA by Perdew, Burke, and Ernzerhof (PBE)[49] to evaluate the KS wave functions and eigenvalues. For more details concerning the HF implementation within the VASP code, we refer to Ref. 50.

Technical details concerning the evaluation of the ACFDT correlation energy will be addressed in more detail in the following. If the RPA is applied, as done in the present work, the integration over the coupling constant λ in Eq. (2) can be performed analytically by employing the respective Dyson equation [Eq. (4)], and the RPA-ACFDT energy can then be expressed as[33]

TABLE II. Atomization energies (kcal/mol) for $H_2$, $N_2$, and $O_2$ from standard DFT-PBE calculations (PBE) and from ACFDT calculations applying the RPA (RPA). Additionally, the contributions to the total ACFDT atomization energy from the ACFDT correlation (Corr.) and from the HF energy (HF) are shown.

| | | PBE | HF | Corr. | RPA | Expt.[a] |
|---|---|---|---|---|---|---|
| $H_2$ | Present | 105 | 84 | 25 | 109 | 109 |
| | Ref. 12 | 105 | 84 | 25 | 109 | |
| $N_2$ | Present | 244 | 111 | 113 | 224 | 228 |
| | Ref. 12 | 244 | 111 | 112 | 223 | |
| $O_2$ | Present | 143 | 25 | 88 | 113 | 121 |
| | Ref. 12 | 144 | 25 | 88 | 113 | |

[a]Reference 51.

$$E_c = \int_0^\infty \frac{d\omega}{2\pi} \mathrm{Tr}\{\ln[1 - \chi^0(i\omega)\nu] + \chi^0(i\omega)\nu\}. \quad (6)$$

For the calculation of the independent-particle response function $\chi^0_{\mathbf{G}'\mathbf{G}}(\mathbf{q}, i\omega)$, one-electron wave functions and eigenvalues of a large number of virtual KS orbitals are needed. We calculate all virtual orbitals spanned by the plane-wave basis set by exact diagonalization of the KS Hamiltonian. The number of filled and empty orbitals is therefore equivalent to the size of the plane-wave basis set, which is, in turn, restricted by the energy cutoff $E_{\text{cut}}$.

Furthermore, the resulting ACFDT correlation energies will depend on the length of the maximum reciprocal lattice vector $G^\chi_{\text{cut}}$ and the energy of the maximum reciprocal lattice vector $E^\chi_{\text{cut}} = (G^\chi_{\text{cut}})^2/2$, respectively. These quantities determine the rank of the tensor $\chi^0_{\mathbf{G}'\mathbf{G}}(\mathbf{q}, i\omega)$ [see Eq. (5)]. The convergence of the RPA-ACFDT correlation energy with $E^\chi_{\text{cut}}$ is slow. However, its functional form can be determined by approximating the independent-particle response function at high $\mathbf{G}$ values by the respective free electron response function. Since this function is known analytically—it is the well known Lindhard function[8]—it is straightforward to calculate the correlation energy for this functional form for different maximum reciprocal lattice vectors $G^\chi_{\text{cut}}$ numerically. For sufficiently large $G^\chi_{\text{cut}}$, we find that the correlation energy behaves as

$$E_c(G^\chi_{\text{cut}}) = E_c^\infty + \frac{A}{(G^\chi_{\text{cut}})^3} = E_c^\infty + \frac{A'}{(E^\chi_{\text{cut}})^{3/2}}, \quad (7)$$

where $E_c^\infty$, $A$, and $A'$ are constants. For the evaluation of the molecular binding energies and the energy-volume curves of the noble gas crystals, we therefore performed calculations for a set of $E^\chi_{\text{cut}} < E_{\text{cut}}$ (typically, $E^\chi_{\text{cut}} < 2/3 E_{\text{cut}}$) and extrapolated to $E_c^\infty := E_c(G^\chi_{\text{cut}} \to \infty)$. The slow convergence with respect to the number of bands and cutoff for the reciprocal lattice vectors is inherent to every plane-wave implementation of the ACFDT. A slightly different procedure than ours was chosen by García-González *et al.*[22] They calculated correlation energies by simultaneously increasing the number of bands and reciprocal lattice vectors and extrapolated these values.

Finally, the frequency integration is performed using a Gauss-Legendre integration. The frequency points, at which Eq. (6) is evaluated, are chosen such that the Gauss-Legendre integration reproduces exact values for an exponentially decaying function. For the noble gas solids, 12 frequency points and a maximal frequency of $\omega_{\text{max}} = 800$ eV result in equilibrium cohesive energies that are converged to within 1 meV. Compared to the case of the noble gas solids, the frequency integrand of the molecules reveals more structure in the low frequency range. This can be ascribed to contributions from transitions between levels with relatively small energy differences, nonexistent in the noble gas solids with their large gap. We found it therefore favorable to increase the density of the frequency grid in the low frequency range when calculating the ACFDT energies for the molecular systems. This was realized by a frequency grid, which for a finite number of points, reproduces exactly the integral of a

function $f(x) \propto x^{(1-B)/B} \exp(-x^{1/B})$. With 16 frequency points, $\omega_{\max}=800$ eV, and $B=1.8$, the error of the molecular ACFDT energies with respect to the frequency integration is again smaller than 1 meV.

## III. COMPUTATIONAL COST

Two parts of the ACFDT correlation energy routines determine the computational requirements of the calculations. First, the response function $\chi^0_{\mathbf{GG}'}(\mathbf{q}, i\omega)$ has to be set up [see Eq. (5)]. This step scales as $N_k^2 N_o N_v (N_{PW}^{\chi})^2$; hence, the scaling is quadratic with respect to the number of $k$ points $N_k$, linear with respect to the number of occupied (virtual) bands $N_o$ ($N_v$) and quadratic with respect to the rank of the response function tensor $N_{PW}^{\chi}$, which is determined by the energy $E_{\text{cut}}^{\chi}$. Second, the evaluation of the integrand in Eq. (6) involves a diagonalization of the response function tensor, which scales like $N_k (N_{PW}^{\chi})^3$. Both computational steps imply a $V^3$ volume scaling for a fixed number of $k$ points and electrons. Obviously, the rank of the response function matrix $N_{PW}^{\chi}$ mainly determines the computational requirements of the ACFDT calculations. It is clearly advantageous to introduce a cutoff for the response function $E_{\text{cut}}^{\chi}$ since this reduces the computational requirements drastically in both the set up of the matrix $\chi$ and the manipulation and diagonalization of the response matrix. In combination with the applied extrapolation to $E_c^{\infty}$, the strategy is also more accurate than a straightforward evaluation of $E_c$ at a specific cutoff, e.g., the naive choice to use the same basis set for the plane-wave expansion of the wave functions and the response function.

## IV. ADIABATIC CONNECTION FLUCTUATION-DISSIPATION THEOREM CALCULATIONS FOR MOLECULES

For the calculation of absolute cohesive energies and heats of formation, it is essential to have the possibility to calculate ACFDT energies both for finite systems such as atoms or molecules and for extended bulk (or surface) systems within one and the same formalism. Most of the ACFDT calculations so far have been performed for molecular systems using local basis set codes.[7,12,16–19] Additionally, Fuchs and co-workers calculated ACFDT energies for atoms and molecules ($H_2$, He, and $Be_2$) within a plane-wave framework.[14,15] A periodic implementation of the ACFDT routines has been applied to the investigation of extended systems (Si/Na in Ref. 20, $h$-BN in Ref. 21, and Si/NaCl in Ref. 22).

In the present work, we perform RPA-ACFDT calculations for molecules and atoms utilizing a plane-wave basis set. As a molecular test set, $H_2$, $N_2$, and $O_2$ were chosen; they have already been investigated by Furche using a local basis set code.[12] The KS one-electron wave functions and energies needed as input to the ACFDT and HF calculations have been calculated using the PBE functional.

For the determination of the standard DFT-PBE atomization energies and the evaluation of the HF energy, we have chosen an energy cutoff as high as $E_{\text{cut}}=1000$ eV. Aspherical contributions to the electrostatic energy as well as to the exchange and (DFT)-correlation energy within the PAW spheres were taken into account. Atoms and molecules have been placed in a cubic supercell with side length 10 Å for $H_2$, $N_2$, and $O_2$, resulting in atomization energies that are converged to within $5\times10^{-2}$ kcal/mol with respect to the supercell volume.

Calculations of ACFDT correlation energies for localized systems within a plane-wave representation are costly due to the large supercells required to avoid interactions between repeated images. The computational time to calculate the RPA-ACFDT correlation energy scales like the cube of the supercell volume (see Sec. III). The largest cell employed is a $7\times7\times7$ Å cell. The cutoff energy $E_{\text{cut}}$ for all considered molecules was set to 600 eV, and the rank of the response function was restrained by using reciprocal lattice vectors with energies smaller than $E_{\text{cut}}^{\chi}=200$, 250, 300, and 350 eV. Atomization energies for $E_{\text{cut}}^{\chi}\to\infty$ were approximated by applying Eq. (7) to the energies obtained for the two largest values of $E_{\text{cut}}^{\chi}$. The cutoff and volume-extrapolated atomization energies for our set of molecules are presented in Table II. They are found to be in excellent agreement with the values calculated by Furche[12] using a local basis set code.

The convergence of the correlation energy with respect to the rank of the response function determined by $E_{\text{cut}}^{\chi}$ and the volume of the supercell is addressed in Fig. 1 for the case of the $N_2$ molecule. The difference of the correlation energy $\Delta E_c = E_c^{N_2} - 2E_c^{N}$ (circles) is plotted versus $E_{\text{cut}}^{\chi}$ for different supercell volumes characterized by their lattice constants. The chosen $(E_{\text{cut}}^{\chi})^{-3/2}$ scale [see Eq. (7)] allows us to fit $\Delta E_c$ for the largest values of $E_{\text{cut}}^{\chi}$ to a straight line and to estimate the extrapolated value $E_{\text{cut}}^{\chi}\to\infty$. If these extrapolated values are plotted against the volumes of the respective supercells, a $V^{-2}$ volume dependence is observed (see the second panel in Fig. 1). The origin of the $\Delta E_c$ increase with the volume of the supercell is related to the long-range $V^{-2}$ vdW interaction between repeated $N_2$ molecules and N atoms. This interaction stabilizes the molecular "crystal," so that for all molecules $\Delta E_c$ tends to be slightly below the respective values found by Furche.[12] For instance, for the $(7\text{ Å})^3$ supercell, the $E_{\text{cut}}^{\chi}$ extrapolated value for $\Delta E_c$ is $-113.3$ kcal/mol; without the artificial interaction between molecules in repeated supercells, $\Delta E_c$ decreases to $-112.5$ kcal/mol (see Table II). For oxygen, the difference between the $(7\text{ Å})^3$ atomization energy ($-88.1$ kcal/mol) and the volume-extrapolated result ($-87.8$ kcal/mol) is slightly smaller.

## V. ADIABATIC CONNECTION FLUCTUATION-DISSIPATION THEOREM FOR NOBLE GAS SOLIDS

In the present work, we calculate the energy-volume curves for the Ne, Ar, and Kr fcc crystals applying the ACFDT formalism within the random phase approximation. The DFT wave functions (wave functions and eigenenergies) needed as input for the HF (ACFDT correlation) energies have been calculated using either the LDA or the PBE approximation for the DFT exchange-correlation potential. The specific choice of the DFT exchange-correlation potential should lead to only small changes in the ACFDT energy, at least for the long-range vdW interaction (see arguments by

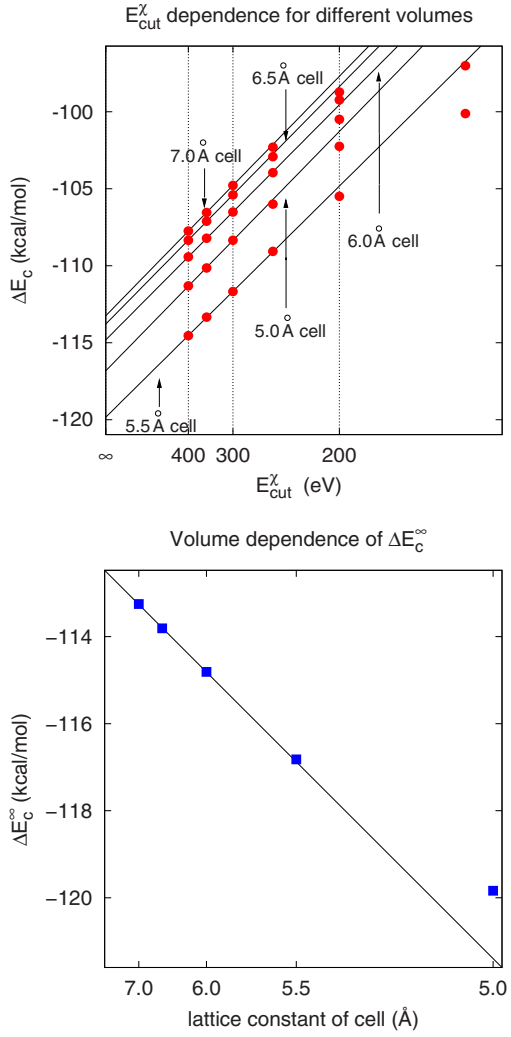


FIG. 1. (Color online) Dependence of the $N_2$ correlation energy difference ($\Delta E_c = E_c^{N_2} - 2E_c^N$) on the energy $E_{cut}^{\chi}$, which determines the rank of the response function matrix [$(E_{cut}^{\chi})^{-3/2}$ scale]. Shown are results for different supercell volumes (circles) and the fit to $E_{cut}^{\chi}$=350 and 300 eV (solid lines). The volume dependence of the extrapolated values $\Delta E_c^{\infty}$ is displayed in the second panel ($V^{-2}$ scale).

Dobson in Ref. 52). Nevertheless, due to the small energies encountered in the noble gas solids, these changes are of the same order as the cohesive energies.

Because the cohesive energies for the noble gas crystals are very small and the minima shallow, all parameters that enter the evaluation of the HF energy and the ACFDT correlation energy have to be carefully tested. In order to achieve smoothness for the HF energy-volume curves on the considered energy scale, the energy cutoff $E_{cut}$ has to be chosen as high as 900 eV for Ne, 390 eV for Ar, and 340 eV for Kr. The $k$-point dependence has been shown to be a critical issue when determining the volume dependence of the HF energies (see also Refs. 21 and 22). Only when using grids as dense as $12\times12\times12$ $k$ points can convergence of the cohesive energies to within 2 meV be achieved.

For the ACFDT correlation energy we found that a $6\times6\times6$ $k$-point set yields already converged and relatively

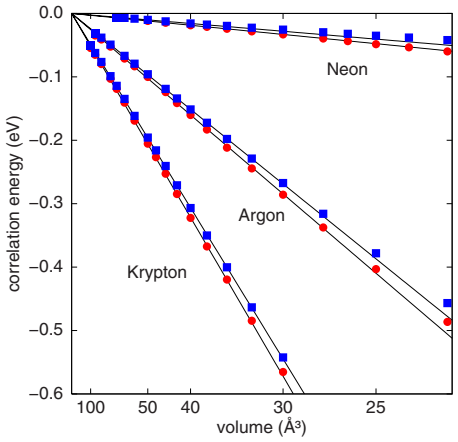


FIG. 2. (Color online) ACFDT correlation energy based on LDA (circles) and GGA-PBE (squares) wave functions and eigenenergies plotted over $1/V^2$. Values are given with respect to the extrapolated correlation energy of the isolated atom.

smooth energy-volume curves. Additionally, the energy cutoff $E_{cut}$ can be reduced from 900 to 650 eV for Ne. The ACFDT correlation energies also depend on the energy $E_{cut}^{\chi}$, which determines the rank of the response function tensor $\chi_{GG'}$. In order to enable extrapolation to infinite values of $E_{cut}^{\chi}$ [see Eq. (7)], a set of $E_{cut}^{\chi}$ has been chosen for each noble gas solid. For Ar and Kr, energy-volume curves have been calculated for $E_{cut}^{\chi}$=175, 200, and 225 eV and for Ne using $E_{cut}^{\chi}$=225, 250, 275, and 300 eV. The differences between cohesive energies determined at the largest value of $E_{cut}^{\chi}$ and the extrapolated energies are as large as 10 meV for Kr and 2 meV for Ne.

In order to determine absolute cohesive energies, the HF energy and the ACFDT correlation energy of the isolated noble gas atoms have to be evaluated as well. The HF energies are calculated by placing a noble gas atom in a supercell and increasing the supercell extension until convergence is reached. Such a direct approach is, in principle and within a certain accuracy, also possible for the ACFDT correlation energy, as has been shown in the previous section. Nevertheless, to achieve accuracy on the 1 meV scale, as needed in the case of the noble gas crystals, the supercell approach becomes cumbersome. Therefore, we evaluate the ACFDT correlation energies of the isolated noble gas atoms by extrapolating the correlation energies from the fcc crystal data. The dependence of the long-range correlation energy on the volume $V$ is known to behave as $1/V^2$—the typical vdW interaction. Indeed, the correlation energies calculated from ACFDT reproduce this functional form exactly. In Fig. 2, the ACFDT correlation energies for Ne, Ar, and Kr based on LDA (circles) and GGA-PBE (squares) wave functions and eigenvalues are shown for different volumes of the fcc cell. The energies are plotted relative to the correlation energy of the isolated noble gas atom obtained when fitting the energy for large volumes to a $1/V^2$ behavior (see Table IV for values of the slope). The quadratic dependence on the volume $V$ holds already for volumes as small as 30 Å$^3$. The uncertainty due to the fit and, consequently, the error bars for the cohesive energy are $\pm2$ meV for Ar and Kr, and $\pm1$ meV for Ne.

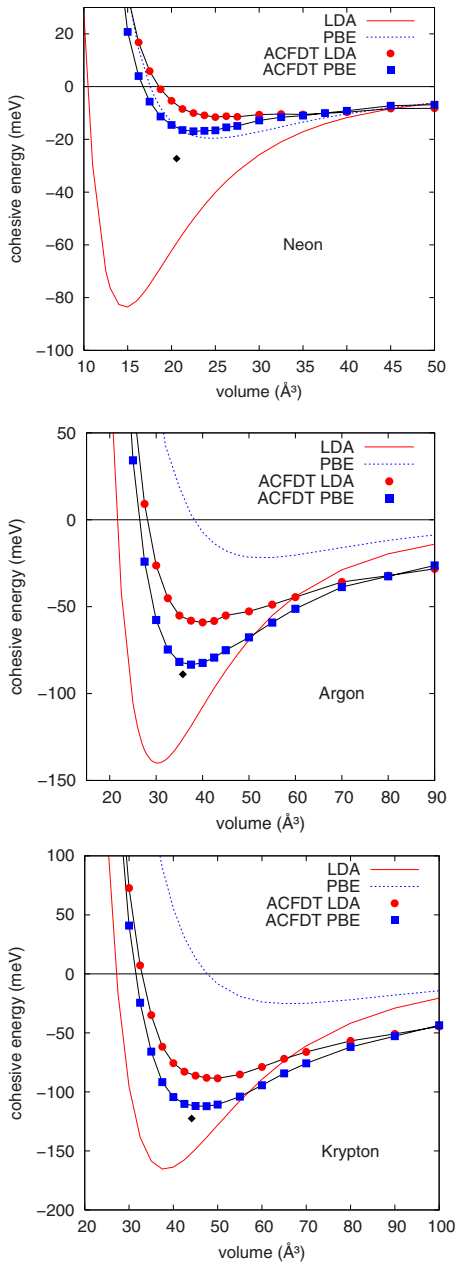


FIG. 3. (Color online) Cohesive energies (meV) as a function of the volume of the primitive cell (Å$^3$) for the fcc noble gas crystals Ne, Ar, and Kr. Besides the cohesive energies obtained from ACFDT calculations based on LDA (circles) and GGA-PBE (squares) wave functions and eigenvalues, standard DFT results within the LDA (solid line) and the PBE (dashed line) are shown. The experimental values (without zero-point energy) are given by black diamonds.

In Fig. 3, the energy-volume curves calculated applying the RPA-ACFDT are shown together with results obtained from standard DFT calculations utilizing the LDA (solid line) and the GGA-PBE (dashed line). Absolute ACFDT energies are determined as described above. The cohesive energies and equilibrium lattice constants are summarized in Table III.

TABLE III. Equilibrium lattice constants and cohesive energies of the noble gas fcc crystals Ne, Ar, and Kr. The DFT results are compared with RPA-ACFDT values and experiment. The zero-point energy is neglected, and the experimental lattice constants are extrapolated to zero temperature (see Ref. 30).

| | DFT-LDA | ACFDT-LDA | DFT-PBE | ACFDT-PBE | Expt. | Ref. 30 |
|---|---|---|---|---|---|---|
| | | | Lattice constant (Å) | | | |
| Ne | 3.9 | 4.7 | 4.6 | 4.5 | 4.35 | 4.314 |
| Ar | 4.9 | 5.4 | 6.0 | 5.3 | 5.23 | 5.284 |
| Kr | 5.3 | 5.8 | 6.4 | 5.7 | 5.61 | 5.670 |
| | | | Cohesive energy (meV) | | | |
| Ne | 83 | 11 | 20 | 17 | 27.3 | 26.44 |
| Ar | 140 | 59 | 22 | 83 | 88.9 | 82.81 |
| Kr | 165 | 88 | 25 | 112 | 122.5 | 114.44 |

For all noble gas solids, standard DFT applying the LDA exchange-correlation potential predicts drastically too large equilibrium cohesive energies at too small equilibrium volumes. Although the relative deviation from experiment decreases for the heavier noble gas solids, even for Kr the cohesive energy is still 40 meV too large. On the other hand, PBE leads to an underbinding with sizable differences from experiment for Ne, Ar, and Kr. The DFT-PBE equilibrium lattice constants are generally much too large.

The RPA-ACFDT using DFT-LDA (circles) or DFT-PBE (squares) one-electron wave functions and eigenvalues consistently improves the equilibrium cohesive energies and lattice constants for Ar and Kr. Especially, the ACFDT-PBE results are in good agreement with experiment: The equilibrium cohesive energy of Kr is calculated to be within 9% of experiment, whereas DFT-LDA overestimates this energy by 35% and DFT-PBE underestimates it by 80%. The deviation from experiment is slightly larger for the ACFDT-LDA calculations. The differences in the cohesive energy between ACFDT-LDA and ACFDT-PBE are 24, 24, and 3 meV for Kr, Ar, and Ne, respectively. Although these differences are small in absolute values, due to the weak binding of the noble gas solids the relative deviations are still significant. In contrast, the RPA-ACFDT equilibrium lattice constants are almost unaffected by the exchange-correlation potential applied in the DFT calculations.

To understand the difference between ACFDT based on LDA and PBE, we show in Fig. 4 the HF and ACFDT correlation energies based on LDA and PBE separately for the Kr crystal. Both contributions are influenced by the choice of the exchange-correlation potential in the KS calculations. For the RPA-ACFDT correlation energy, the RPA response function of the separated subsystems determines the strength of the long-range correlation effects (see Ref. 31). Generally, the PBE leads to a weaker response than the LDA and, consequently, to smaller long-range correlation energies. For the noble gas solids, this fact is best observed in Fig. 2. However, the larger part of the LDA/PBE deviation stems from

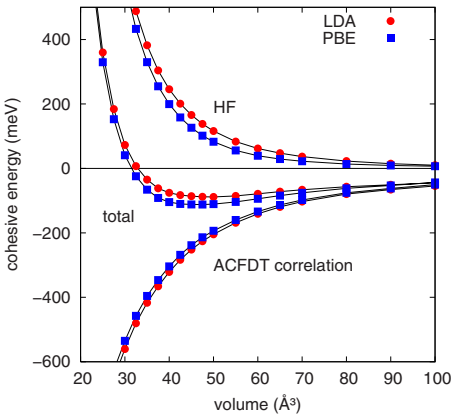


FIG. 4. (Color online) Kr total ACFDT cohesive energies and contributions arising from the HF and the ACFDT correlation energy calculations. Energies based on DFT-LDA (circles) and DFT-PBE (squares) wave functions and eigenenergies are shown.

the HF Hamiltonian evaluated using LDA/PBE wave functions, with a general trend to smaller HF energies for DFT-PBE wave functions. This implies a closer resemblance of the PBE KS wave functions to the groundstate HF wavefunctions.

We also evaluated energy-volume curves within the RPA+.[13] The absolute equilibrium cohesive energies are 10 meV (2 meV) smaller for Kr (Ne) than the respective RPA values, therefore moving further away from the experimental values.

## VI. DISCUSSION AND CONCLUSION

The description of vdW bonded systems exposes one of the basic limitations of KS density functional theory within the LDA and GGA. Both LDA and GGA rely on a local or semi-local exchange-correlation potential and are hence not capable to predict the correct long-range interaction between subsystems with nonoverlapping densities. The ACFDT provides a post-DFT approach that relies on the DFT wave functions and eigenenergies but includes exact exchange and a compatible correlation energy that is calculated from the nonlocal response function. In order to evaluate the response function of the interacting system, the exchange-correlation kernel in the Dyson equation, which relates the interacting to the noninteracting response function, has to be approximated. However, even within the RPA, where the exchange-correlation kernel is set to zero and only Hartree effects are included, the ACFDT should yield at least qualitatively the correct vdW behavior.

In this paper, we have reported on RPA-ACFDT total energy calculations for the fcc noble gas solids Ne, Ar, and Kr. We found that the RPA-ACFDT leads to an improved description of the equilibrium cohesive energies and lattice constants for Ar and Kr, with a general trend to underbinding at slightly too large equilibrium lattice constants. The final results are a clear improvement over semilocal density functionals. For Ne, the ACFDT results are not quite as good and the predicted equilibrium properties show only a slight improvement over conventional DFT-PBE. With respect to the starting functionals, we find similar results for LDA and PBE, with the latter always yielding stronger binding and better agreement with experiment. Astonishingly, the difference between ACFDT-PBE and ACFDT-LDA is largely dominated by differences in the Hartree-Fock contributions, with ACFDT-PBE yielding a stronger binding than ACFDT-LDA through that contribution. We believe that this is related to a more accurate description of the decay of the one-electron potentials in PBE and a concomitant improved description of the decay of the one-electron wave functions.

TABLE IV. $C_6$ (eV Å$^6$) coefficients for the noble gas solids, where $C_6$ determines the strength of the long-range $C_6/r_0^6$ interaction ($r_0$ is the nearest neighbor distance). This value equals twice the slopes of the curves shown in Fig. 2. The "experimental" values are estimated by fitting the experimental zero-point corrected equilibrium energies and equilibrium volumes (Ref. 30) to a Lennard-Jones pair potential (Ref. 30).

| | Expt. | LDA | PBE |
|---|---|---|---|
| Ne | 47 | 62 | 53 |
| Ar | 455 | 512 | 484 |
| Kr | 895 | 1030 | 980 |

The contributions to the correlation energy also differ for LDA and PBE, but the difference is in the opposite direction: Now, the LDA yields a stronger binding contribution than the PBE, so that the net results are fairly independent of the starting functional. To discuss this point quantitatively, Table IV summarizes the attractive $1/r^6$ coefficients $C_6$ determined from the theoretical long-range part of the correlation energy (see Fig. 2). It is not straightforward to compare these values with experiment. However, Rościszewski *et al.* reported experimental binding energies and experimental volumes corrected for zero point fluctuations.[30] From those values, we have extracted the "experimental" $C_6$ coefficients, assuming a simple pairwise Lennard-Jones potential. The agreement with experiment is indeed rather satisfactory, particularly on the GGA-PBE level. A slight overestimation for all three noble gas solids is clearly visible, which could be related to the fact that local and semilocal functionals generally yield somewhat too large polarizabilities, the LDA more so than the GGA-PBE. Actually, the macroscopic dielectric constants of fcc Ar at the experimental equilibrium volume are 1.705 and 1.661 for LDA and PBE, respectively (Ne: 1.251 and 1.249; Kr: 1.895 and 1.838), and hence consistently larger for LDA than GGA, in line with the previous argument. We also note that the inclusion of an exchange-correlation kernel in the calculation of the response function of the interacting system always increases the polarizability, which will most likely further worsen the agreement with experiment.

The good agreement of the GGA $C_6$ coefficients with experiment indicates that discrepancies for the equilibrium volume and binding energies are most likely related to deficiencies at short and medium bond distances, where the Pauli repulsion becomes important. At these bond distances, the correlation energy and the repulsive Hartree-Fock energy (evaluated using the Kohn-Sham wave functions) contribute

equally, but with opposite signs, to the energy. As discussed, the wave functions have a large influence on the Hartree-Fock energy contribution at this bond length, and it is conceivable that errors are dominated by errors in the wave functions. Clearly, however, exchange and correlation energies are most difficult to describe at intermediate bond distances rather than at long distances.

Finally, we presented atomization energies for $H_2$, $N_2$, and $O_2$. The atomization energies are within 1 kcal/mol, identical to those obtained by Furche,[12] confirming the ability of the present plane-wave basis set implementation to calculate very accurate ACFDT energies also for molecules and atoms. Admittedly, plane waves are not the ideal choice for such calculations since the treatment of vacuum is rather expensive, and the calculational cost increases with the cube of the supercell volume $V^3$. Nevertheless, the presented calculations suggest that we can obtain equally reliable total energies for extended and finite systems using plane waves and carefully constructed PAW potentials. How well ACFDT works for extended solid state systems with chemical bonding will be the subject of a forthcoming publication.

## ACKNOWLEDGMENT

This work was supported by the Austrian *Fonds zur Förderung der wissenschaftlichen Forschung* (FWF) under Grant No. Y218 (START).

*georg.kresse@univie.ac.at

[1] W. Kohn and L. J. Sham, Phys. Rev. **140**, A1133 (1965).
[2] A. Seidl, A. Görling, P. Vogl, J. A. Majewski, and M. Levy, Phys. Rev. B **53**, 3764 (1996).
[3] D. C. Langreth and J. P. Perdew, Solid State Commun. **17**, 1425 (1975).
[4] O. Gunnarsson and B. I. Lundqvist, Phys. Rev. B **13**, 4274 (1976).
[5] D. C. Langreth and J. P. Perdew, Phys. Rev. B **15**, 2884 (1977).
[6] A. Klein, Phys. Rev. **121**, 950 (1961).
[7] N. E. Dahlen, R. van Leeuwen, and U. von Barth, Int. J. Quantum Chem. **101**, 512 (2005).
[8] U. von Barth and L. Hedin, J. Phys. C **5**, 1629 (1972).
[9] J. Harris and A. Griffin, Phys. Rev. B **11**, 3669 (1975).
[10] J. M. Pitarke and A. G. Eguiluz, Phys. Rev. B **57**, 6329 (1998).
[11] J. F. Dobson and J. Wang, Phys. Rev. Lett. **82**, 2123 (1999).
[12] F. Furche, Phys. Rev. B **64**, 195120 (2001).
[13] S. Kurth and J. P. Perdew, Phys. Rev. B **59**, 10461 (1999).
[14] M. Fuchs and X. Gonze, Phys. Rev. B **65**, 235109 (2002).
[15] M. Fuchs, Y. M. Niquet, X. Gonze, and K. Burke, J. Chem. Phys. **122**, 094116 (2005).
[16] F. Furche and T. Voorhis, J. Chem. Phys. **122**, 164106 (2005).
[17] F. Aryasetiawan, T. Miyake, and K. Terakura, Phys. Rev. Lett. **88**, 166401 (2002); **90**, 189702 (2003).
[18] N. E. Dahlen and U. von Barth, Phys. Rev. B **69**, 195102 (2004).
[19] N. E. Dahlen, R. van Leeuwen, and U. von Barth, Phys. Rev. A **73**, 012511 (2006).
[20] T. Miyake, F. Aryasetiawan, T. Kotani, M. van Schilfgaarde, M. Usuda, and K. Terakura, Phys. Rev. B **66**, 245103 (2002).
[21] A. Marini, P. García-González, and A. Rubio, Phys. Rev. Lett. **96**, 136404 (2006).
[22] P. García-González, J. J. Fernández, A. Marini, and A. Rubio, J. Phys. Chem. A **111**, 12458 (2007).
[23] Y. Andersson, D. C. Langreth, and B. I. Lundqvist, Phys. Rev. Lett. **76**, 102 (1996).
[24] M. Lein, J. F. Dobson, and E. K. U. Gross, J. Comput. Chem. **20**, 12 (1999).
[25] M. Dion, H. Rydberg, E. Schröder, D. C. Langreth, and B. I. Lundqvist, Phys. Rev. Lett. **92**, 246401 (2004).
[26] J. G. Ángyán, I. C. Gerber, A. Savin, and J. Toulouse, Phys. Rev. A **72**, 012510 (2005).
[27] F. Ortmann, F. Bechstedt, and W. G. Schmidt, Phys. Rev. B **73**, 205101 (2006).
[28] P. Schwerdtfeger, N. Gaston, R. P. Krawczyk, R. Tonner, and G. E. Moyano, Phys. Rev. B **73**, 064112 (2006).
[29] I. C. Gerber and J. G. Ángyán, J. Chem. Phys. **126**, 044103 (2007).
[30] K. Rościszewski, B. Paulus, P. Fulde, and H. Stoll, Phys. Rev. B **60**, 7905 (1999).
[31] J. F. Dobson, K. McLennan, A. Rubio, J. Wang, T. Gould, H. M. Le, and B. P. Dinte, Aust. J. Chem. **54**, 513 (2001).
[32] J. F. Dobson, A. White, and A. Rubio, Phys. Rev. Lett. **96**, 073201 (2006).
[33] Y. M. Niquet, M. Fuchs, and X. Gonze, Phys. Rev. A **68**, 032507 (2003).
[34] J. F. Dobson, in *Topics in Condensed Matter*, edited by M. P. Das (Nove, New York, 1994).
[35] E. Runge and E. K. U. Gross, Phys. Rev. Lett. **52**, 997 (1984).
[36] E. K. U. Gross and W. Kohn, Phys. Rev. Lett. **55**, 2850 (1985).
[37] J. P. Perdew and Y. Wang, Phys. Rev. B **45**, 13244 (1992).
[38] M. Lein, E. K. U. Gross, and J. P. Perdew, Phys. Rev. B **61**, 13431 (2000).
[39] J. Jung, P. García-González, J. F. Dobson, and R. W. Godby, Phys. Rev. B **70**, 205107 (2004).
[40] S. L. Adler, Phys. Rev. **126**, 413 (1962).
[41] N. Wiser, Phys. Rev. **129**, 62 (1963).
[42] G. Kresse and J. Hafner, Phys. Rev. B **48**, 13115 (1993).
[43] G. Kresse and J. Furthmüller, Comput. Mater. Sci. **6**, 15 (1996).
[44] P. E. Blöchl, Phys. Rev. B **50**, 17953 (1994).
[45] G. Kresse and D. Joubert, Phys. Rev. B **59**, 1758 (1999).
[46] M. Gajdoš, K. Hummer, G. Kresse, J. Furthmüller, and F. Bechstedt, Phys. Rev. B **73**, 045112 (2006).
[47] M. Shishkin and G. Kresse, Phys. Rev. B **74**, 035101 (2006).
[48] J. Harl and G. Kresse (unpublished).
[49] J. P. Perdew, K. Burke, and M. Ernzerhof, Phys. Rev. Lett. **77**, 3865 (1996).
[50] J. Paier, R. Hirschl, M. Marsman, and G. Kresse, J. Chem. Phys. **122**, 234102 (2005).
[51] K. P. Huber and G. Herzberg, *Constants of Diatomic Molecules*, Molecular Spectra and Molecular Structure Vol. IV (Van Nostrand Reinhold, New York, 1979).
[52] J. F. Dobson, *Time-Dependent Density Functional Theory*, edited by M. A. L. Marques, C. A. Ullrich, F. Noqueira, A. Rubio, K. Burke, and E. K. U. Gross (Springer, Berlin, 2006).